Journal of Thermal Analysis, Vol. 52 (1998) 853-862

THERMAL STABILITY STUDY OF Fe–Ni-BASED ALLOYS Determination of T–HR–T and T–T–T diagrams

J. J. Suñol[1], *N. Clavaguera*[2] *and M. T. Mora*[3]

[1]Departamento Enginyeria Industrial, Universitat de Girona, E-17071 Girona
[2]Departamento ECM, Facultade Física, Universitat de Barcelona, E-08028 Barcelona
[3]Grup de Física de Materials I, Univ. Autònoma de Barcelona, E-08193 Bellaterra, Spain

Abstract

The low-temperature parts of the temperature–heating rate–transformation (T–HR–T) and temperature-time transformation (T–T–T) diagrams were obtained for crystallization processes. A knowledge of the kinetic model governing crystallization is not needed because both transformation curves can be obtained from non-isothermal calorimetric experiments. The calorimetric study was performed by means of differential scanning calorimetry. The method was applied to analyse crystallization processes of Fe–Ni-based amorphous alloys prepared by melt spinning. The compositions studied were $Fe_{40}Ni_{40}P_{14}Si_6$, $Fe_{40}Ni_{40}P_{10}Si_{10}$ and $Fe_{40}Ni_{40}P_6Si_{14}$.

A good concordance was oberved between the experimental T–HR–T curves obtained by calculation and the experimental data, which verifies the reliability of the method. In the T–T–T diagrams, the agreement was good in process Bl, while in processes Al and Cl there are small differences that could be related to different crystallization products obtained in isothermal/non-isothermal experiments.

Keywords: crystallization, DSC, melt spinning, T–HR–T diagrams, T–T–T diagrams

Introduction

Temperature–heating rate–transformation (T–HR–T) and temperature–time transformation (T–T–T) diagrams are very useful for predicting the transformation that may occur on controlled non-isothermal or isothermal treatment of a material. A knowledge of thermal stability is important to control the structure (and properties) of the materials. For instance, processes such as crystallization promote changes in material properties.

Reactions inside materials frequently display great complexity. During the crystallization process, several phases form and then disappear almost simultaneously. The calorimeter records then relative to overlapping processes and hence kinetic models governing crystallization can not be deduced. Nevertheless, it may still be possible to construct T–HR–T and T–T–T diagrams [1, 2]. In

1418–2874/98/ $ 5.00

Akadémiai Kiadó, Budapest
Kluwer Academic Publishers, Dordrecht

our case to illustrate both the advantages and the limitations of this method, it was applied to the crystallization of Fe Ni based amorphous alloys prepared by melt spinning.

The field of rapid solidification of metals and alloys from the liquid state has undergone enormous progress during the last three decades. This started with the successful rapid quenching experiments of Falkenhagen [3] and Duwez [4, 5], where different extended solid solutions were obtained. Recently, rapid quenching techniques have attracted considerable interest because a large number of metastable materials, such as amorphous phases, extended solid solutions and non-equilibrium crystalline phases, have been produced. The large-scale production of continuous ribbons made of Fe-, Ni- or Co-based soft magnetic amorphous alloys has already been achieved.

Metallic glasses are being used in various applications because their properties are often significantly better than those of their conventional counterparts [6]. Not much has been written about the quaternary system Fe–Ni–P–Si analysed in this study. Nevertheless, there are some references to its thermal stability, compared to that of alloys with identical nominal composition obtained by mechanical alloying [7, 8]. T–HR–T and T–T–T allow the control of thermal stability and the prevention of crystallization processes that produce drastic changes in the mechanical and magnetic properties of materials.

Experimental

Polycrystalline elemental Fe, Ni, P and Si, and alloy Fe–P (25 at%) were used as precursors to obtain amorphous-like alloys with the following nominal compositions: $Fe_{40}Ni_{40}P_{14}Si_6$, $Fe_{40}Ni_{40}P_{10}Si_{10}$ and $Fe_{40}Ni_{40}P_6Si_{14}$, denoted as A, B and C, respectively.

The melt spinning equipment consisted of a copper wheel, a quartz crucible with an orifice containing the alloy and a coil connected to an RF generator. The alloy sample, about 4 g in mass, was melted under an argon atmosphere. The wheel surface velocity was 30 m s^{-1}. The working conditions of the device were chosen so that the alloys could be obtained in an amorphous state and in ribbon form.

The calorimetric experiments were carried out in a DSC7 Perkin Elmer calorimeter under an inert argon atmosphere. Thermal stability was analysed via isothermal and non-isothermal experiments. Isothermal measurements were performed at a heating rate of 300 K min^{-1} until the annealing temperature was reached. The experiments at constant heating rate were recorded from room temperature up to temperature, above the crystallization exotherms, at scan rates ranging from 5 to 80 K min^{-1}.

Crystallization kinetics

To explain the thermal behaviour on crystallization, each crystallization step is assumed to have a rate of transformation given by

$$\frac{d\alpha}{dt} = k(T)f(\alpha) \tag{1}$$

where α is the fraction crystallized at time t and temperature T, $k(T)$ is the rate constant and $f(\alpha)$ is a function that reflects the limiting mechanism of crystallization. These functions are assumed to be independent of the thermal history of the sample [9–11]. It is expected that $k(T)$ could exhibit simple Arrhenius behaviour i.e.

$$k(T) = k_o \exp\left(-\frac{E}{RT}\right) \tag{2}$$

where k_o is the pre-exponential factor and E is the apparent activation energy, both quantities assumed to be practically independent of temperature, at least in the temperature interval accessible in the calorimetric measurements.

Several methods can be applied to obtain the activation energy in non-isothermal measurements. In our work, the Kissinger peak method [12] has been applied. This involves the assumption that at the maximum peak temperatures, $(d^2\alpha/dt^2)_{T=Tp}=0$. This condition can be rewritten in terms of the constant heating rate β and the activation energy

$$\ln\left(\frac{\beta}{T_p^2}\right) = -\frac{E}{RT_p} + C \tag{3}$$

where C is a smooth function of α which can be assumed to be constant for moderate values of β [13].

Under isothermal conditions, Eq. (1) can be integrated to give

$$g(\alpha) = \int_0^\alpha \frac{d\alpha}{f(\alpha)} = k_o \exp\left(-\frac{E}{RT}\right) t \tag{4}$$

This equation, when represented as temperature *vs.* the time needed for crystallization of a fixed fraction, α, of the material, gives the T–T–T curve.

By the same procedure, integration of Eq. (1) under constant rate temperature variation, β, gives

$$g(\alpha) = \int_0^{\alpha} \frac{d\alpha}{f(\alpha)} = \frac{k_0}{\beta} \int \exp\left(-\frac{E}{RT}\right) dT \tag{5}$$

The solution obtained can be represented in a diagram that shows the temperature at which a certain amount of crystalline material will we obtained on heating/cooling as a function of the heating/cooling rate. Such diagrams are the temperature–heating/cooling rate– transformation or T–HR/CR–T curves [14].

Usually, the values for the crystallization process that are obtainable from DSC experiments [15, 16] and which are essential in the empirical determination of the low-temperature parts of the T–T–T and T–HR–T curves are the activation energy and $k_0 f(\alpha)$.

Once the value of E is known, it is usual to evaluate the function $f(\alpha)$ from the continuous heating experiments and to compare the value obtained with that obtained in the isothermal experiments [17]. Nevertheless, in our case overlapping crystallization processes occur simultaneously and a kinetic model governing crystallization can not be deduced correctly. However, a method of obtaining T–HR–T and T–T–T diagrams from non-isothermal data can be applied. T–HR–T curves can be obtained by integration from Eq. (1):

$$\beta = \frac{k_0 R T^2 \exp\left(-\frac{E}{RT}\right)}{E \int_0^{\alpha} \frac{d\alpha}{f(\alpha)}} \tag{6}$$

and T–T–T curves can be obtained from

$$t = \exp\left(-\frac{E}{RT}\right) \int_0^{\alpha} \frac{d\alpha}{k_0 f(\alpha)} \tag{7}$$

By using the following equation, one can solve the integral of Eqs (6) and (7) even if the value of $f(\alpha)$ is unknown:

$$\int_0^{\alpha} \frac{d\alpha}{k_0 f(\alpha)} = \int_0^{T} \frac{\exp\left(\frac{E}{RT}\right)}{\beta} dT \tag{8}$$

To calculate T–HR–T and T–T–T diagrams, it is necessary to solve the right integral of Eq. (8); the only experimental data are one calorimetric curve and the activation energy of the process.

Application to Fe–Ni-based alloys

In the quenched ribbons, complete amorphization was achieved. Mössbauer spectroscopy, X-ray diffraction and transmission electron microscopy measurements confirmed this [1]. The calorimetric analysis demonstrated the presence of two exothermic crystallization processes (denoted as 1 and 2) in each of the three ribbons. Accordingly, the processes were denoted as A1-A2, B1-B2 and C1-C2 in ribbons A, B and C, respectively. The main one, process 1, was that with lower

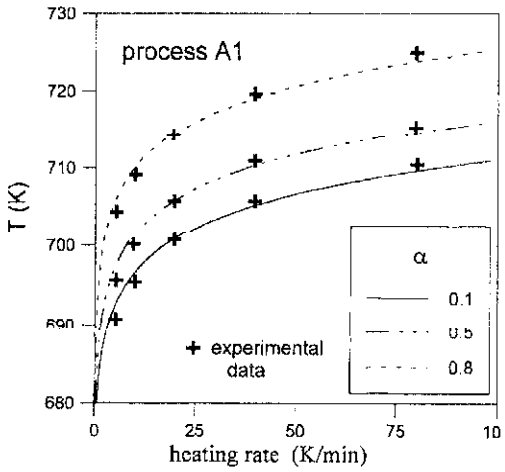

Fig. 1 Low-temperature part of the T–HR–T diagram; $Fe_{40}Ni_{40}P_{14}Si_6$ ribbon alloy; Process A1

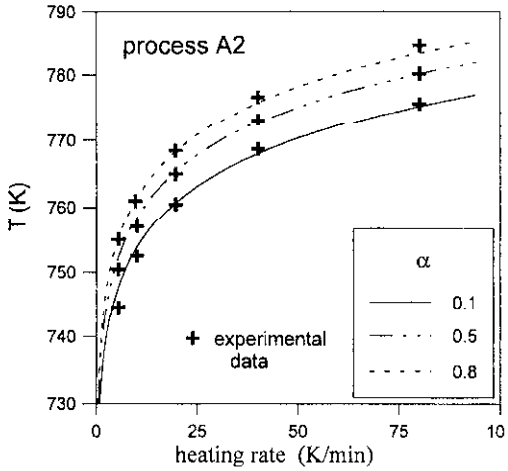

Fig. 2 Low-temperature part of the T–HR–T diagram; $Fe_{40}Ni_{40}P_{14}Si_6$ ribbon alloy; Process A2

temperature, which appeared when the temperature was higher than 650 K. The second process started when the temperature was beyond 740 K. The activation energy of the main/second peak ranged from 640/470 to 290/160 kJ mol^{-1}; similar values were obtained in Fe–Ni-based alloys obtained by mechanical alloying [18, 19]. Via Eqs (6) and (7), T–HR–T and T–T–T diagrams were calculated. The experimental data used to construct these were one calorimetric curve (in this study that corresponding to a heating rate of 20 K min^{-1}) and the activation energy.

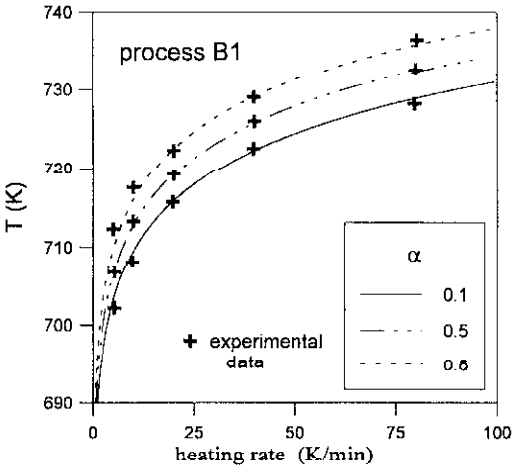

Fig. 3 Low-temperature part of the T–HR–T diagram; $Fe_{40}Ni_{40}P_{10}Si_{10}$ ribbon alloy; Process B1

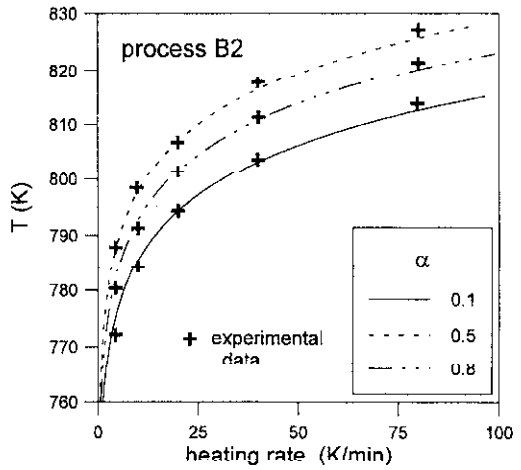

Fig. 4 Low-temperature part of the T–HR–T diagram; $Fe_{40}Ni_{40}P_{10}Si_{10}$ ribbon alloy; Process B2

Figures 1–6 show the T–HR–T curves calculated with the experimental data that correspond to α values of 0.1, 0.5 and 0.8. Curves were compared with the experimental data from measurements at other heating rates to check the methodological validity. The results correlated well, which verifies the reliability of the method utilised. The major application of the T–HR–T curves is for prediction of the amount of material crystallized during treatment of the samples at a certain constant heating rate.

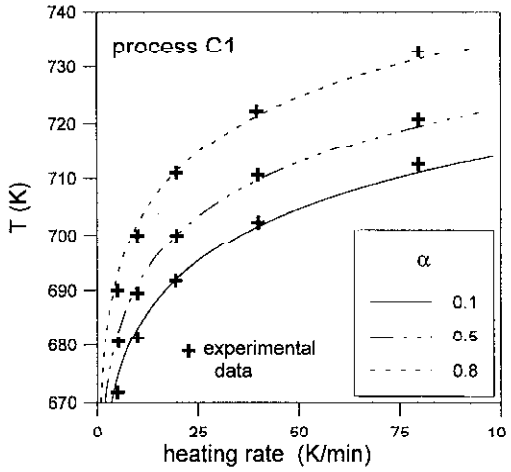

Fig. 5 Low-temperature part of the T–HR–T diagram; $Fe_{40}Ni_{40}P_6Si_{14}$ ribbon alloy; Process C1

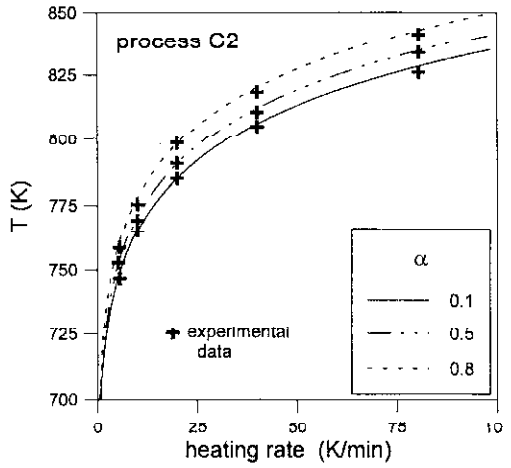

Fig. 6 Low-temperature part of the T–HR–T diagram; $Fe_{40}Ni_{40}P_6Si_{14}$ ribbon alloy; Process C2

Figures 7–9 show the T–T–T curves of processes A1, B1 and C1 respectively. In a very similar way to the T–HR–T case, the curves obtained were compared with experimental isothermal data. The agreement was good in process B1, but several differences appear for processes A1 and C1. Perhaps different products of crystallization were obtained from isothermal and non-isothermal treatments. The coupling of calorimetric and structural studies would be of interest.

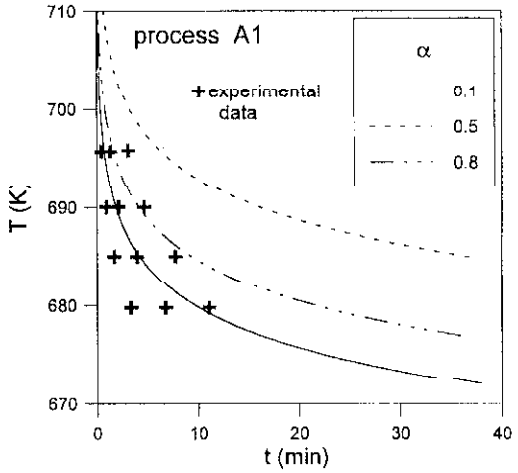

Fig. 7 Low-temperature part of the T–T–T diagram; $Fe_{40}Ni_{40}P_{14}Si_6$ ribbon alloy; Process A1

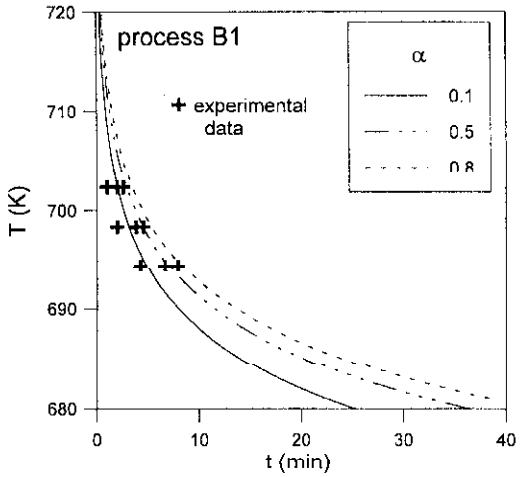

Fig. 8 Low-temperature part of the T–T–T diagram; $Fe_{40}Ni_{40}P_{10}Si_{10}$ ribbon alloy; Process B1

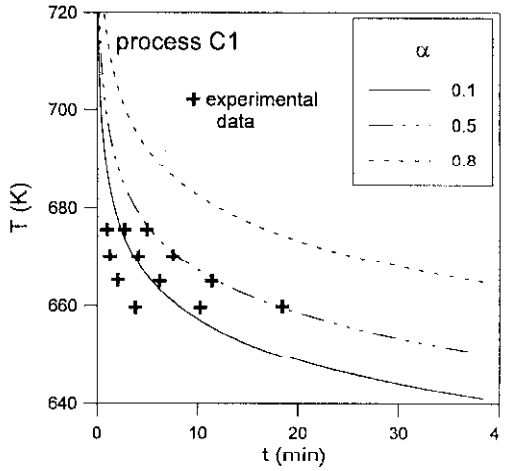

Fig. 9 Low-temperature part of the T–T–T diagram; $Fe_{40}Ni_{40}P_6Si_{14}$ ribbon alloy; Process C1

Conclusions

The low-temperature parts of the temperature–heating rate–transformation (T–HR–T) and temperature–time–transformation (T–T–T) diagrams were obtained for crystallization processes. Both transformation curves could be obtained from one non-isothermal calorimetric experiment and the activation energy. The method was applied to analyse crystallization processes of Fe–Ni-based amorphous alloys prepared by melt spinning. A good concordance was observed between the experimental T–HR–T curves obtained by calculation and the experimental data, which verifies the reliability of the method. In the T T T diagrams, the agreement was good in process B1, while in processes A1 and C1 there are small differences that could be related to different crystallization products obtained in isothermal/non-isothermal experiments. The activation energies of the crystallization processes ranged from 640 to 160 kJ mol^{-1}.

* * *

This work was supported in part by a grant from the CIRIT (GRQ-2048), which we gratefully acknowledge.

References

1 J. J. Suñol, Ph. D. Thesis, Universitat Autonoma de Barcelona (1996).
2 Zhu Jie, Ph. D. Thesis, Universitat Autónoma de Barcelona (1996).
3 G. Falkenhagen and W. Hoffman, Z. Metallk., (1952) 69.
4 P. Duwez, R. H. Willens and W. Kelemnt, J. Appl. Phys., (1960) 1136.

5 P. Duwez, W. Klement and R. H. Willens, Nature, 186 (1960) 869.
6 H. J. Güntherodt, Rapidly Quenched Metals, Elsevier Science Publishers, (1985).
7 T. Pradell, N. Clavaguera, J. J. Suñol and M. T. Mora, ICAME95, Rimini, (1995) 433.
8 M. T. Mora, J. J. Suñol and N. Clavaguera, in 'Nanostructured and non-crystalline materials', eds. M. Vázquez and H. Hernando, World Scientific (1995) 44.
9 D. W. Henderson, J. Non-Crystalline Solids, 30 (1979) 301.
10 J. Šesták and G. Berggren, Thermochim. Acta, 3 (1971) 1.
11 H. S. Chen, J. Non-Cryst. Solids, 27 (1978) 257.
12 H. E. Kissinger, Anal. Chem., 29 (1957) 1702.
13 M. D. Baró, N. Clavaguera, S. Bordas, M. T. Mora and J. Casas-Vazquez, J. Thermal Anal., 11 (1977) 1213.
14 M. T. Mora, S. Suriñach, M. D. Baró and N. Clavaguera, Solid State Ionics, 63–65 (1993) 268.
15 S. Suriñach, M. D. Baró, M. T. Mora and N. Clavaguera, J. Non-Cryst. Solids, 58 (1983) 209.
16 M. T. Mora, S. Suriñach, M. D. Baró, A. Otero and N. Clavaguera, Thermochim. Acta, 203 (1992) 379.
17 S. Bordas, M. T. Mora and N. Clavaguera, Journal of Non-Cryst. Solids, 119 (1990) 232.
18 M. T. Mora, S. Suriñach, M. D. Baró, J. Segura, J. J. Suñol and N. Clavaguera, Bol. Soc. Esp. Cer y Vid., 31-C (1992) 369.
19 S. Suriñach, J. J. Suñol and M. D. Baró, Materials Science and Engineering A181/A182 (1994) 1285–1290.